Provably Robust Semi-Infinite Program Under Collision Constraints via Subdivision

Duo Zhang, Xifeng Gao, Kui Wu, and Zherong Pan

Abstract—We present a semi-infinite program (SIP) solver for trajectory optimizations of general articulated robots. These problems are more challenging than standard Nonlinear Program (NLP) by involving an infinite number of non-convex, collision constraints. Prior SIP solvers based on constraint sampling cannot guarantee the satisfaction of all constraints. Instead, our method uses a conservative bound on articulated body motions to ensure the solution feasibility throughout the optimization procedure. We further use subdivision to adaptively reduce the error in conservative motion estimation. Combined, we prove that our SIP solver guarantees feasibility while approaches the critical point of SIP problems up to arbitrary user-provided precision. We have verified our method on a row of trajectory optimization problems involving industrial robot arms and UAVs, where our method can generate collision-free, locally optimal trajectories within a couple minutes.

Index Terms—Semi-Infinite Program, Trajectory Optimization, Collision Handling, Articulated Body

I. INTRODUCTION

This paper deals with trajectory generation for articulated robots, which is a fundamental problem in robotic motion planning. Among other requirements, providing strict collision-free guarantees is crucial to a robust algorithm, i.e., the robot body should be bounded away from static and dynamic obstacles by a safe distance at any time instance. In addition to robustness, modern planning algorithms such as [1] further seek (local) optimality, i.e., finding trajectories that correspond to the minimizers of user-specified cost functions. Typical cost functions would account for smoothness [2], energy efficacy [3], time-optimization [4], and etc. Despite decades of research, achieving simultaneous robustness and optimality remains a challenging problem.

There are two notable categories of techniques that attempt to generate robust and optimal trajectories. Sampling-based motion planners [5] and their optimal variants [6] explore potential robot motions and then check the motion safety by sampling at discrete time instances, for which efficient discrete collision detection (DCD) algorithms [7] can be used. However, insufficient sampling resolutions can miss infeasible constraints and compromise their robustness. This problem is partially remedied by continuous collision detection (CCD) [8, 9, 10, 11, 12], which is capable of finding the first time-of-impact within a continuous time interval. However, CCD assumes simple object shapes under linear or affine motions, which cannot be generalized to arbitrary articulated motions, i.e. the end-effector motion of a robot arm.

Optimal sampling-based methods are a kind of zeroth-order optimization algorithm that does not use gradient information to guide trajectory search. In parallel, first- and second-order

Duo Zhang, Xifeng Gao, Kui Wu, and Zherong Pan are with the Lightspeed Studios, Tencent. {zduozhang, xifgao, kwwu, zrpan@global.tencent.com}

trajectory optimization algorithms [13] have been proposed to utilize derivative information to bring the trajectory towards a local minimizer. Despite the efficacy of high-order techniques, dealing with collision constraints becomes a major challenge as the number of constraints is infinite, leading to SIP problems [14]. To the best of our knowledge, all the existing trajectory optimizers for articulated robots are based on the exchange method [15], i.e., sampling the constraints at discrete time instances. Similar to the DCD algorithms used in the sampling-based method, the exchange method can miss infeasible constraints and sacrifice the robustness guarantee.

We propose a novel SIP solver with guaranteed robustness. Our method is based on the discretization method [15]. Conceptually, our discretization method resembles the CCD algorithm used in sampling-based motion planners. We divide a robot trajectory into intervals and use conservative motion bound to ensure the collision-free property during each interval. These intervals further introduce barrier penalty functions, which guide the optimizer to stay inside the feasible domain and approach the optimal solution of SIP problems up to arbitrary user-specified precision. The key components of our method involve: 1) a motion bound that conservatively estimates the range of motion of a point on the robot over a finite time interval; 2) a safe line-search algorithm that prevents the intersection between the motion bound and obstacles; 3) a motion subdivision scheme that recursively reduces the error of conservative motion estimation. By carefully designing the motion bound and line search algorithm, we prove that our solver converges within finitely many iterations. We have also evaluated our method on a row of examples, including industrial robot arms reaching targets through complex environments and multi-UAV trajectory generation with simultaneous rotation and translation. Our method can generate safe trajectories within a couple of minutes on a single desktop machine.

II. RELATED WORK

We review related works in SIP and its application in robotics, continuous collision avoidance, and collision-free trajectory generation.

SIP models mathematical programs involving a finite number of decision variables but an infinite number of constraints. SIP frequently arises in robotic applications for modeling constraints on motion safety [14, 16], controllability and stability [17, 18], reachability [19], and pervasive contact realizability [20]. The key challenge of solving SIP lies in the reduction of the infinite constraint set to a computable finite set. Such reduction has been well-studied in several special cases. The controllability of a linear dynamic system at any continuous time instance can be verified by checking

the rank of the controllability matrix. It is also well-known that a positive semi-definite cone is equivalent to an infinite number of linear constraints [21]. The more general sum-of-squares program [22] ensures the positivity of a polynomial on a semi-algebraic set. However, these techniques impose strong assumption on the constraint formulation or restrict the solution to a small subset of the feasible domain. In parallel, general-purpose SIP solvers have been proposed that impose much weaker assumption on the constraint formulations [15], such as linearity, convexity, and differentiability, of which two representative methods are the exchange and discretization method. Both methods perform the finite reduction via sampling and then solve the finite subproblem as a conventional nonlinear program (NLP). However, even starting from a feasible initial point, these methods cannot guarantee the feasibility of solutions. Instead, we propose a feasible discretization method for solving the special SIP under collision constraints, which guarantees both the feasibility and optimality of solutions. Our method is inspired by the exact penalty formulation [23, 24], which reduces the SIP to a conventional NLP by integrating over the constraint indices. We further approximate such integrals by subdivision and show that our approximation is tractable to compute while preserving both the feasibility and optimality of solutions.

Continuous collision avoidance is one of the most fundamental capabilities of a robot system. Unfortunately, even verifying the collision-free property over a continuous domain or along a continuous trajectory is a challenging problem. For simple object shapes under linear or affine motions, geometric rules have been developed for check continuous collisions [10, 11, 12], but they cannot be generalized to arbitrary nonlinear motions. For robots governed by polynomial dynamic systems, a Control Barrier Function (CBF) [25, 26] can be designed to avoid continuous collisions against known obstacles. Amice *et al.* [16] recently proposed an optimization-based formulation to identify positive-measure, collision-free configuration subsets for arbitrary articulated robots. Unlike these techniques that only satisfy the continuous collision constraints, we aim at optimizing a trajectory under these constraints. A closely related work to ours is [27], which uses the Taylor series to estimate the range of motion and check for collision conservatively. We use such conservative estimation to ensure that each step of optimization stays inside the feasible domain.

Collision-free trajectory generation is a kind of SIP problem that computes an optimal robot trajectory that has no collision with the environment or against other robots at any continuous time instance. To this end, most existing techniques [1, 28, 29, 30] formulate the problem as a numerical optimization under collision constraints. However, all these methods use infeasible algorithms as the underlying solver, relying on the gradient information to push an infeasible solution back into the feasible domain. Such a push-back procedure is not guaranteed to succeed, especially when either the robot or the environment contains geometrically thin objects [1, 14]. Even worsen, these methods sample the collision constraints at finite intervals, potentially leading to arbitrarily large feasibility errors. As a special case, when the robot can be approximated as a point, and its trajectory is piecewise
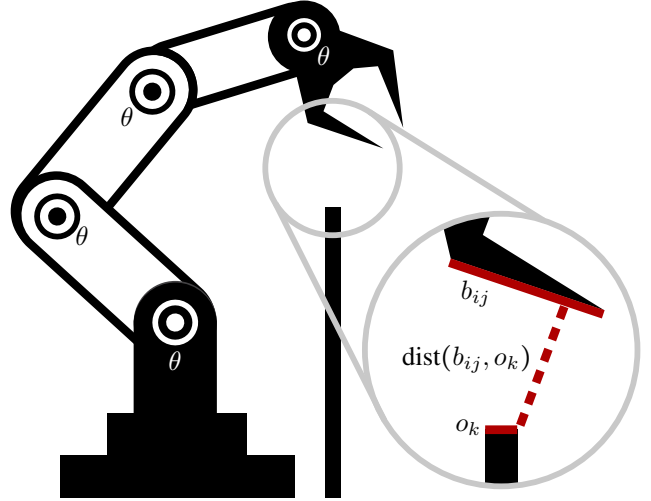

Fig. 1: We consider a moving articulated robot arm, where the volume occupied by the ith link is denoted as b_i. Each b_i endows a finite decomposition $b_i = \bigcup_j b_{ij}$ and each b_{ij} is a simple shape, e.g. the red edge. b_{ij} is a function of the time t and trajectory parameters θ, denoted as $b_{ij}(t, \theta)$. θ could be the control points of Bézier curves in the configuration space. Similarly, we can decompose the obstacle $o = \bigcup_k o_k$ where o_k is the short red edge. We introduce log barrier energy bounding the distance $\text{dist}(b_{ij}, o_k)$ (dashed line) away from a safety distance d_0.

polynomial, the SIP endows a disjointly convex relaxation [31] allowing globally optimal solutions to be found via mixed-integer programs. But such relaxation is not available for more general kinematic systems such as articulated robots. In parallel, optimal sampling-based motion planner [5, 6] searches for piecewise linear trajectories in a robot's configuration space, while the corresponding workspace trajectories can still be arbitrarily complex and their collision-free properties need to be checked via sampling.

III. PROBLEM STATEMENT

In this section, we provide a general formulation for collision-constrained trajectory generation problems. Throughout the paper, we will use subscripts to index geometric entities or functions, but we choose not to indicate the total number of indices to keep the paper succinct, e.g., we denote $\sum_i$ as a summation over all indices i. We consider an open-loop articulated robot as composed of several rigid bodies. The ith rigid body occupies a finite volume in the global frame, denoted as $b_i \subset \mathbb{R}^3$. Without ambiguity, we refer to the rigid body and its volume interchangeably. We further denote $b_i^0 \subset \mathbb{R}^3$ as the volume of ith body in its local frame. We further assume there is a set of static obstacles taking up another volume $o \in \mathbb{R}^3$. By the articulated body kinematics, we can compute b_i from b_i^0 via the rigid transform: $b_i = M_i b_i^0$ where we define $M_i b_i^0 = \{M_i x | x \in b_i^0\}$. When a robot moves, M_i and thus b_i are time-dependent functions, denoted as $M_i(t, \theta)$ and $b_i(t, \theta)$, respectively. Here $t \in [0, T]$ is the time parameter and the trajectory is parameterized by a set

of decision variables, denoted as θ. The problem of collision-constrained trajectory generation aims at minimizing a twice-differentiable cost function $\mathcal{O}(b_i)$, such that each rigid body b_i is bounded away from o by a user-specified safe distance denoted as d_0 at any $t \in [0, T]$. Formally, this is defined as:

$$\underset{\theta}{\operatorname{argmin}} \; \mathcal{O}(b_i(t, \theta))$$
$$\text{s.t.} \quad \operatorname{dist}(b_i(t, \theta), o) \geq d_0 \quad \forall i \wedge t \in [0, T], \quad (1)$$

where $\operatorname{dist}(\bullet)$ is the shortest Euclidean distance between two sets. The cost function $\mathcal{O}(b_i(t, \theta))$ can encode various user requirements for a "good" trajectory, i.e., the the closedness between an end-effector and a target position, or the smoothness of motion. This is a SIP due to the infinitely many constraints, one corresponding to each time instance. Further, the SIP is non-smooth as the distance function between two general sets is non-differentiable. Equation (1) is a general definition incorporating various geometric representations of the robot and obstacles as illustrated in Figure 1.

A. Smooth Approximation

Although the main idea of this work is a discretization method for solving Equation (1), most existing SIP solvers already adopt the idea of discretization for spatial representation of a rigid body b_i to deal with non-smoothness of the function $\operatorname{dist}(\bullet)$. By spatial discretization, we assume that b_i endows a finite decomposition $b_i = \bigcup_j b_{ij}$ where b_{ij} is the jth subset of b_i in world frame. Similarly, we can finitely decompose o as $o = \bigcup_k o_k$ where o_k is the kth subset of environmental obstacles o in the world frame. If the distance function $\operatorname{dist}(b_{ij}, o_k)$ between a pair of subsets is differentiable, then we can reduce the non-smooth SIP Equation (1) to the following smooth SIP:

$$\underset{\theta}{\operatorname{argmin}} \; \mathcal{O}(b_i(t, \theta))$$
$$\text{s.t.} \quad \operatorname{dist}(b_{ij}(t, \theta), o_k) \geq d_0 \quad \forall i, j, k \wedge t \in [0, T]. \quad (2)$$

In summary, spatial discretization is based on the following assumption:

Assumption III.1. *Each b_i and o endows a finite decomposition denoted as $b_i = \bigcup_j b_{ij}$ and $o = \bigcup_k o_k$ such that $\operatorname{dist}(b_{ij}, o_k)$ is sufficiently smooth for any $\langle i, j, k \rangle$.*

The two common spatial discretization methods are point cloud and triangle mesh. In the case of point cloud, each b_{ij} or o_k is a point, and dist is the differentiable pointwise distance. In the case of the triangle mesh, it has been shown that the distance between a pair of triangles can be reduced to two sub-cases: 1) the distance between a point and a triangle and 2) the distance between a pair of edges, both of which are twice differentiable after slight bulging [32]. We will further show in Section VI that the distance between a pair of convex hulls can also be made twice differentiable. Although spatial discretization can generate many more distance constraints, only a few constraints in close proximity to each other need to be activated and forwarded to the SIP solver for consideration, and these potentially active constraints can be efficiently identified using a spatial acceleration data structure [33]. Despite
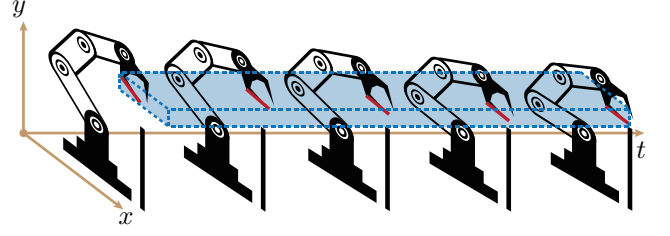

Fig. 2: When the red edge illustrated in Figure 1 is tracing out a temporal trajectory, we use a spatial-temporal motion bound (blue) to estimate its range and guarantee safety.

these spatial discretizations, however, the total number of constraints is still infinite in the temporal domain.

B. The Exchange Method

The exchange method is a classical algorithm for solving general SIP that has been adopted in [14] to solve Equation (1). This method reduces SIP to a series of NLP by sampling constraints both spatially and temporally. Specifically, the algorithm maintains an instance set $\mathcal{I}$ that contains a finite set of $\langle i, j, k, t \rangle$ tuples and reduces Equation (1) to the following NLP:

$$\underset{\theta}{\operatorname{argmin}} \; \mathcal{O}(b_i(t, \theta))$$
$$\text{s.t.} \quad \operatorname{dist}(b_{ij}(t, \theta), o_k) \geq d_0 \quad \forall \langle i, j, k, t \rangle \in \mathcal{I}. \quad (3)$$

The algorithm approaches the solution of Equation (1) by alternating between solving Equation (3) and updating $\mathcal{I}$. The success of the exchange method relies on a constraint selection oracle for updating $\mathcal{I}$. Although several heuristic oracles are empirically effective, we are unaware of any exchange method that can guarantee the satisfaction of semi-infinite constraints. Indeed, most exchange methods insert new $\langle i, j, k, t \rangle$ pairs into $\mathcal{I}$ when the constraint is already violated, aka. $\operatorname{dist}(b_{ij}(t, \theta), o_k) < d_0$, and relies on the underlying NLP solver to pull the solution back onto the constrained manifold, where the feasibility guarantee is lost. In practice, the exchange method can fail when dealing with geometrically thin objects with ill-defined gradient information [1, 14].

IV. SUBDIVISION-BASED SIP SOLVER

We propose a novel subdivision-based SIP solver inspired by the discretization method [15]. Unlike the exchange method that selects the instance set $\mathcal{I}$ using an oracle algorithm, the discretization method uniformly subdivides the index set into finite intervals and chooses a surrogate index from each interval to form the instance set $\mathcal{I}$, reducing the original problem into an NLP. As a key point of departure from the conventional infeasible discretization method, however, we design the surrogate constraint in Section IV-A such that its feasible domain is a strict subset of the true feasible domain of Equation (1). We then show in Section IV-B and Section IV-C that, by using feasible interior point method such as [34] to solve the NLP, our algorithm is guaranteed to generate iterations satisfying all the surrogate constraints. Since our surrogate constraint can limit the solution to an

overly conservative subset, in Section IV-D, we introduce a subdivision method to adaptively adjust the conservative subset and approach the original feasible domain.

A. Surrogate Constraint

We consider the following infinite spatial-temporal subset of constraints:

$$\text{dist}(b_{ij}(t,\theta), o_k) \geq d_0 \quad \forall t \in [T_0, T_1] \subseteq [0, T], \quad (4)$$

where b_{ij} and o_k are two spatial subsets and $[T_0, T_1] \subseteq [0, T]$ is a temporal subset. Our surrogate constraint replaces the entire time interval with a single time instance. A natural choice is to use the following midpoint constraint:

$$\text{dist}\left(b_{ij}\left(\frac{T_0 + T_1}{2}, \theta\right), o_k\right) \geq d_0, \quad (5)$$

which is differentiable by Assumption III.1. Unfortunately, the domain specified by Equation (5) is larger than that of Equation (4), violating our feasibility requirement. We remedy this problem by upper-bounding the feasibility error due to the use of our surrogate. A linear upper bound can be established by taking the following mild assumption:

Assumption IV.1. *The feasible domain of t and θ is bounded.*

Lemma IV.2. *Under Assumption III.1, IV.1, there exists a constant L_1 such that:*

$$|dist(b_{ij}(t_1, \theta), o_k) - dist(b_{ij}(t_2, \theta), o_k)| \leq L_1 |t_1 - t_2|.$$

Proof. A differentiable function in a bounded domain is also Lipschitz continuous so that we can define L_1 as the Lipschitz constant. □

The above result implies that the feasibility error of the midpoint surrogate constraint is upper bounded by $L_1(T_1 - T_0)/2$. Further, the feasible domain is specified by the following more strict constraint:

$$\text{dist}(b_{ij}(t, \theta), o_k) \geq d_0 + L_1 |T_1 - T_0|/2,$$

is a subset of the true feasible domain. However, such a subset can be too restrictive and oftentimes lead to an empty feasible domain. Instead, our method only uses Lemma IV.2 as an additional safety check as illustrated in Figure 2, while the underlying optimizer deals with the standard constraint Equation (5). Note that the bound in Lemma IV.2 is not tight and there are many sophisticated upper bounds that converge superlinearly, of which a well-studied method is the Taylor model [27]. Although we recommend using the Taylor model in the implementation of our method, our theoretical results merely require a linear upper bound.

B. Barrier Penalty Function

To ensure our algorithm generates feasible iterations, we have to solve the NLP using a feasible interior-point method such as [34]. These algorithms turn each inequality collision constraint into the following penalty function:

$$\mathcal{P}_{ijk}(t, \theta) \triangleq \mathcal{P}\left(\text{dist}\left(b_{ij}(t, \theta), o_k\right) - d_0\right),$$

where $\mathcal{P}$ is a sufficiently smooth, monotonically decreasing function defined on $(0, \infty)$ such that $\lim_{x \to 0} \mathcal{P}(x) = \infty$ and $\lim_{x \to \infty} \mathcal{P}(x) = 0$. In order to handle SIP problems, we need the following additional assumption to hold for $\mathcal{P}$:

Assumption IV.3. *The barrier function $\mathcal{P}$ satisfies:*

$$\lim_{x \to 0} x \mathcal{P}(x) = \infty.$$

The most conventional penalty function is the log-barrier function $\mathcal{P}(x) = -\log(x)$, but this function violates Assumption IV.3. By direct verification, one could see that a valid penalty function is $\mathcal{P}(x) = -\log(x)/x$. In [33], authors showed that a locally supported $\mathcal{P}$ is desirable for a spatial acceleration data structure to efficiently prune inactive constraints, for which we propose the following function:

$$\mathcal{P}(x) = \begin{cases} \frac{(x_0 - x)^3}{x^4} & x \leq x_0 \\ 0 & x > x_0, \end{cases}$$
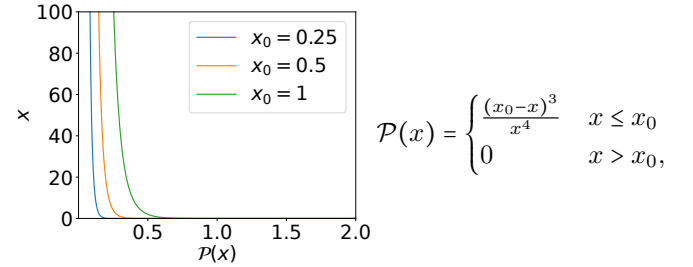
which is twice differentiable and locally supported within $(0, x_0]$ with x_0 being a small positive constant. The intuition behind Assumption IV.3 lies in the integral reformulation of semi-infinite constraints. Indeed, we can transform the infinite constraints into a finite form by integrating the penalty function over semi-infinite variables, giving the following finite integral penalty function, denoted as $\bar{\mathcal{P}}$:

$$\bar{\mathcal{P}}_{ijk}(T_0, T_1, \theta) \triangleq \int_{T_0}^{T_1} \mathcal{P}_{ijk}(t, \theta) dt. \quad (6)$$

The above integral penalty function has been considered in [23, 24, 35] to solve SIP. However, their proposed algorithms are only applicable for special forms of constraints, where the integral in Equation (6) has a closed-form expression. Unfortunately, such an integral in our problem does not have a closed-form solution. Instead, we propose to approximate the integral via spatial-temporal discretization. We will show that the error in our discrete approximation is controllable, which is crucial to the convergence of our proposed solver. In order for the penalty function to guarantee feasibility, $\bar{\mathcal{P}}_{ijk}$ must tend to infinity when:

$$\exists t \in [T_0, T_1] \quad \text{dist}\left(b_{ij}(t, \theta), o_k\right) \to d_0. \quad (7)$$

However, the log-barrier function does not satisfy this property. As illustrated in the inset, suppose there is a straight line trajectory $b_{ij}(t) = (t, 0, 0)$ along the positive X-axis, o is the YZ-plane that intersects the X-axis at $(1/2, 0, 0)$, $T = 1$ and $d_0 = 0$, then $\bar{\mathcal{P}}$ takes the following finite value:

$$\bar{\mathcal{P}}_{ijk}(0, 1) \triangleq \int_0^1 -\log\left(\left|t - \frac{1}{2}\right|\right) dt = \log(2) + 1 < \infty.$$
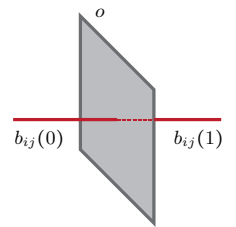
Instead, our Assumption IV.3 could ensure the well-definedness of $\bar{\mathcal{P}}$ as shown in the following lemma:

Lemma IV.4. *Suppose Assumption III.1, IV.3, and Equation* (7) *holds, then:* $\bar{\mathcal{P}}_{ijk} \to \infty$.

Proof. Without loss of generality, we assume $t \in (T_0, T_1)$ so we can pick a positive ϵ_1 such that $[t-\epsilon_1, t+\epsilon_1] \subseteq [T_0, T_1]$. For any $t' \in [t-\epsilon_1, t+\epsilon_1]$, by Assumption III.1 and the boundedness of t', we have:

$$\text{dist}\left(b_{ij}\left(t', \theta\right), o_k\right) \le \text{dist}\left(b_{ij}\left(t, \theta\right), o_k\right) + L_1|t' - t|.$$

Putting things together, we have:

$$\bar{\mathcal{P}}_{ijk}(T_0, T_1, \theta) \ge \bar{\mathcal{P}}_{ijk}(t - \epsilon_1, t + \epsilon_1, \theta)$$
$$\ge \epsilon_1 \mathcal{P}\left(\text{dist}\left(b_{ij}\left(t, \theta\right), o_k\right) - d_0 + L_1\epsilon_1\right) \ge \epsilon_1 \mathcal{P}(\epsilon_1 + L_1\epsilon_1),$$

where the last inequality is due to Equation (7) and by choosing θ so that $\text{dist}\left(b_{ij}\left(t, \theta\right), o_k\right) - d_0 \le \epsilon_1$. The lemma is proved by tending ϵ_1 to zero and applying IV.3. $\quad\square$

C. Feasible Interior-Point Method

We now combine the above ideas to design a feasible interior point method for the SIP problem. We divide the bounded temporal domain into a disjoint set of intervals, $[0, T] = \bigcup_l [T_0^l, T_1^l]$, and choose the midpoint constraint as the representative. As a result, the penalty functions transform the inequality-constrained NLP into an unconstrained one as follows:

$$\underset{\theta}{\arg\min}\ \mathcal{E}(\theta) \triangleq \mathcal{O}(\theta) + \mu \sum_{ijkl} (T_1^l - T_0^l)\mathcal{P}_{ijkl}(\theta)$$
$$\mathcal{P}_{ijkl}(\theta) \triangleq \mathcal{P}_{ijk}\left(\frac{T_0^l + T_1^l}{2}, \theta\right), \tag{8}$$

where μ is a positive weight controlling the duality gap. Note that we weight the penalty function $\mathcal{P}_{ijkl}$ by the time span $T_1^l - T_0^l$ in order to approximate the integral form $\bar{\mathcal{P}}_{ijkl}(\theta) \triangleq \bar{\mathcal{P}}_{ijk}(T_0^l, T_1^l, \theta)$ in the sense of Riemann sum. Standard first- and second-order algorithms can be utilized to solve Equation (8), where the search direction of a first-order method $d^{(1)}$ is:

$$d^{(1)} \triangleq -\nabla_\theta \mathcal{E},$$

and that of the second-order method is:

$$d^{(2)} \triangleq \text{adj}\left(\nabla_\theta^2 \mathcal{E}\right)^{-1} d^{(1)}.$$

Here $\text{adj}(\bullet)$ is an adjustment function for a Hessian matrix such that $\underline{\beta}I \preceq \text{adj}(H) \preceq \bar{\beta}I$ for some positive constants $\underline{\beta}$ and $\bar{\beta}$. After a search direction is computed, a step size α is adaptively selected to ensure the first Wolfe's condition:

$$\mathcal{E}(\theta + d\alpha) \le \mathcal{E}(\theta) + c\langle d\alpha, \nabla_\theta \mathcal{E}\rangle, \tag{9}$$

where $c \in (0, 1)$ is a positive constant. It has been shown that if the smallest $z \in \mathbb{Z}^+$ is chosen such that $\alpha = 1/z$ satisfies Equation (9), then the feasible interior-point method would converge to the first-order critical point of $\mathcal{E}$ [36, Proposition 1.2.4]. Under the finite-precision arithmetic of a computer, we would terminate the loop of θ update when $\|d^{(1)}\|_\infty \le \epsilon_d$. Furthermore, we add an outer loop to reduce the

duality gap by iteratively reducing μ down to a small constant ϵ_μ. The overall interior point procedure of solving inequality-constrained NLP is summarized in Algorithm 1.

Algorithm 1: Feasible Interior Point Method

Input: Feasible θ, initial μ, ϵ_α, ϵ_d, ϵ_μ, $\gamma \in (0, 1)$
Output: Locally optimal θ
1: **while** $\mu > \epsilon_\mu$ **do**
2: $\quad d \leftarrow d^{(1)}$ or $d \leftarrow d^{(2)}$
3: $\quad$ **while** $\|d\|_\infty > \epsilon_d$ **do**
4: $\quad\quad \alpha, \epsilon_\alpha \leftarrow$ Line-Search$(\theta, d, \epsilon_\alpha)$
5: $\quad\quad \theta \leftarrow \theta + d\alpha$
6: $\quad\quad d \leftarrow d^{(1)}$ or $d \leftarrow d^{(2)}$
7: $\quad \mu \leftarrow \mu\gamma$
8: Return θ

D. Adaptive Subdivision

Algorithm 1 is used to solve NLP instead of SIP. As analyzed in Section IV-A, the feasible domain of NLP derived by surrogate constraints can be larger than that of SIP. To ensure feasibility in terms of semi-infinite constraints, we utilize the motion bound Lemma IV.2 and add an additional safety check in the line search procedure as summarized in Algorithm 2. Algorithm 2 uses a more conservative feasibility condition that shrinks the feasible domain by $\psi(T_1^l - T_0^l)$. The motion bound Lemma IV.2 immediately indicates that $\psi(x) = L_1 x/2$. However, our theoretical analysis requires an even more conservative ψ defined as:

$$\psi(x) = L_1 x/2 + L_2 x^\eta, \tag{10}$$

where L_2 and η are positive constants. We choose to only accept α found by the line search algorithm when $\theta + d\alpha$ passes the safety check. On the other hand, the failure of a safety check indicates that the surrogate constraint is not a sufficiently accurate approximation of the semi-infinite constraints and a subdivision is needed. We thus adopt a midpoint subdivision, dividing $[T_0^l, T_1^l]$ into two pieces $[T_0^l, (T_0^l+T_1^l)/2]$ and $[(T_0^l+T_1^l)/2, T_1^l]$. This procedure is repeated until α found by the line search algorithm passes the safety check. Note that the failure of safety check can be due to two different reasons: 1) the step size α is too large; 2) more subdivisions are needed. Since the first reason is easier to check and fix, so we choose to always reduce α when safety check fails, until some lower bound of α is reached. We maintain such a lower bound denoted as ϵ_α. Our line-search method is summarized in Algorithm 3. Our SIP solver is complete by combining Algorithm 1, 2, and 3.

Algorithm 2: Safety-Check(θ)

Output: $\langle i, j, k, l\rangle$ such that $\mathcal{P}_{ijkl}$ violates safety condition
1: **for** Each penalty term $\mathcal{P}_{ijkl}$ **do**
2: $\quad$ **if** $\text{dist}\left(b_{ij}\left(\frac{T_0^l+T_1^l}{2}, \theta\right), o_k\right) \le d_0 + \psi(T_1^l - T_0^l)$ **then**
3: $\quad\quad$ Return $\langle i, j, k, l\rangle$
4: Return None

Algorithm 3: Line-Search($\theta, d, \epsilon_\alpha$)

Input: Initial α_0, $\gamma \in (0,1)$
Output: Step size α and updated ϵ_α

1: $\alpha \leftarrow \alpha_0$
2: $\theta' \leftarrow \theta + d\alpha$
3: $\langle i,j,k,l \rangle \leftarrow$ Safe-Check(θ')
4: **while** $\langle i,j,k,l \rangle \neq$ None $\lor$ θ' violates Equation (9) **do**
5:    **if** $\langle i,j,k,l \rangle \neq$ None **then**
6:       **if** $\alpha \leq \epsilon_\alpha$ **then**
7:          $\epsilon_\alpha \leftarrow \gamma \epsilon_\alpha$
8:          Subdivide($\mathcal{P}_{ijkl}$) and re-evaluate $\mathcal{E}(\theta)$
9:          $d \leftarrow d^{(1)}$ or $d \leftarrow d^{(2)}$
10:       **else**
11:          $\alpha \leftarrow \gamma \alpha$
12:    **else**
13:       $\alpha \leftarrow \gamma \alpha$
14:    $\theta' \leftarrow \theta + d\alpha$
15:    $\langle i,j,k,l \rangle \leftarrow$ Safe-Check(θ')
16: Return α, ϵ_α

V. CONVERGENCE ANALYSIS

In this section, we argue that our Algorithm 1 is suited for solving SIP problems Equation (1) by establishing three properties. First, the following result is straightforward and shows that our algorithm generates feasible iterations:

Theorem V.1. *Under Assumption III.1 and Assumption IV.1, each θ generated by an iteration of Algorithm 1 is a feasible solution to Equation (1).*

Proof. A step size generated by Algorithm 3 must pass the safety check, which in turn ensures that:

$$\text{dist}\left(b_{ij}\left(\frac{T_0^l + T_1^l}{2}, \theta\right), o_k\right)$$
$$\geq d_0 + \psi(T_1 - T_0) > d_0 + L_1 \frac{T_1^l - T_0^l}{2},$$

where we have used our choice of ψ in Equation (10). From Lemma IV.2, we have for any $t \in [T_0^l, T_1^l]$ that:

$$\text{dist}(b_{ij}(t, \theta), o_k)$$
$$\geq \text{dist}\left(b_{ij}\left(\frac{T_0^l + T_1^l}{2}, \theta\right), o_k\right) - L_1 \left| t - \frac{T_0^l + T_1^l}{2} \right| > d_0.$$

Since Algorithm 3 would check every spatial-temporal constraint subset, the proof is complete. $\square$

Theorem V.1 depends on the fact that Algorithm 1 does generate an iteration after a finite amount of computation. However, the finite termination of Algorithm 1 is not obvious for two reasons. First, the line search Algorithm 3 can get stuck in the while loop and never pass the safety check. Second, even if the line search algorithm always terminate finitely, the inner while loop in Algorithm 1 can get stuck forever. This is because a subdivision would remove one and contribute two more penalty terms of form: $(T_1^l - T_0^l)\mathcal{P}_{ijkl}$ to $\mathcal{E}(\theta)$, which changes the landscape of objective function. As a result, it is possible for a subdivision to increase $\|d\|_\infty$ and Algorithm 1

can never bring $\|d\|_\infty$ down to user-specified ϵ_d. However, the following result shows that neither of these two cases would happen by a proper choice of η:

Theorem V.2. *Under Assumption III.1, IV.1, IV.3, and suppose $\eta < 1/6$, Algorithm 1 terminates after a finite number of subdivisions.*

Proof. See Section IX. $\square$

Theorem V.2 shows the well-definedness of Algorithm 1, which aims at solving the NLP Equation (8) instead of the original Equation (1). Our final result bridges the gap by showing that the first-order optimality condition of Equation (8) approaches that of Equation (1) by a sufficiently small choice of μ and ϵ_μ:

Theorem V.3. *We take Assumption III.1, IV.1, IV.3, X.2 and suppose $\eta < 1/6$. If we run Algorithm 1 for infinite number of iterations using null sequences $\{\mu^k\}$ and $\{\epsilon_d^k\}$, where k is the iteration number, then we get a solution sequence $\{\theta^k\}$ such that every accumulation point θ^0 satisfies the first-order optimality condition of Equation (1).*

Proof. See Section X. $\square$

VI. REALIZATION ON ARTICULATED ROBOTS

In this section, we present a practical realization of our method to generate trajectories of articulated robots with translational and hinge rotational joints. We consider two versions of our method. In our first version, we assume both the robot and the environmental geometries are discretized using triangular meshes. In order to ensure collision-free between the two geometric shapes, it is equivalent to ensuring that distance between every edge-edge and vertex-triangle pair is larger than d_0 [37]. In other words, the b_{ij} and o_k can be a moving point, edge, or triangle. Such distance functions have been shown to be twice differentiable after slight bulging [32].

A. Computing Lipschitz Upper Bound

The Lipschitz constant L_1 needs to be evaluated for both the edge-edge and vertex-triangle pairs. We denote by L_1^{ij} as the Lipschitz constant of b_{ij} satisfying Lemma IV.2. We first consider the case with b_{ij} being a moving point, and all other cases are covered by minor modifications. We denote Θ as the vector of joint parameters, which is also a function of t and θ. By the chain rule, we have:

$$L_1^{ij} = \max \left| \frac{\partial \text{dist}(b_{ij}(t,\theta), o_k)}{\partial t} \right|$$
$$= \max \left| \frac{\partial \text{dist}(b_{ij}(t,\theta), o_k)}{\partial b_{ij}(t,\theta)} \frac{\partial b_{ij}(t,\theta)}{\partial \Theta(t,\theta)} \frac{\partial \Theta(t,\theta)}{\partial t} \right|.$$

Without a loss of generality, we assume each entry of $\partial\Theta(t,\theta)/\partial t$ is limited to the range $[-1,1]$. The first term is a distance function, whose subgradient has a norm at most 1 [38]. These results combined, we have:

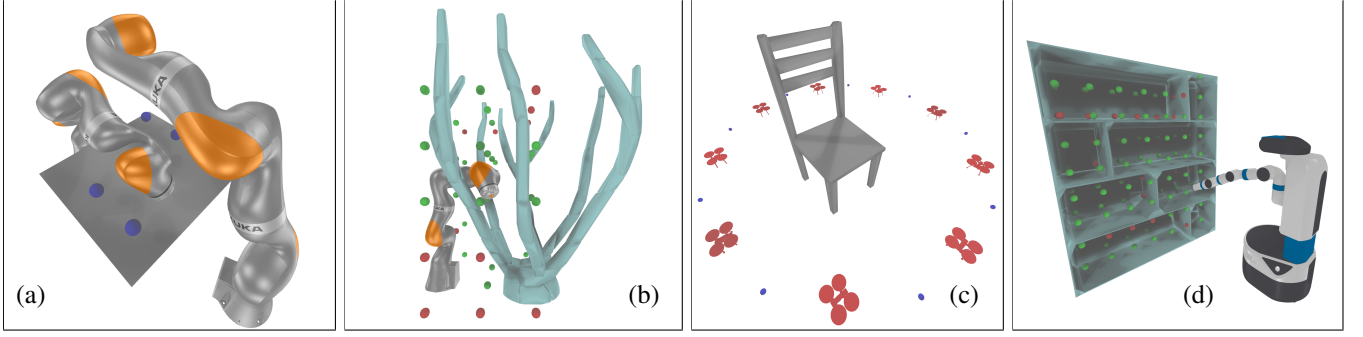$$L_1^{ij} \leq \max \left| \frac{\partial b_{ij}(t,\theta)}{\partial \Theta(t,\theta)} \right|_{2,1},$$

Fig. 3: Snapshots of our four benchmark problems.

which means L_1^{ij} is upper bound of the $2,1$-norm of the Jacobian matrix. Next, we consider the general case with b_{ij} being a triangle with three vertices denoted as $b_{ij}^{1,2,3}$. We have the closest point on b_{ij} to o_k lies on some interpolated point $b_{ij}^1\xi^1 + b_{ij}^2\xi^2 + b_{ij}^3\xi^3$, where $\xi^{1,2,3}$ are interpolation weights that are also function of $\theta(t)$. However, if we fix $\xi^{1,2,3}$ as constants, this would only increase the Lipschitz constant. In other words:

$$\left|\frac{\partial \text{dist}(b_{ij}(t,\theta),o_k)}{\partial t}\right| \le \left|\frac{\partial \text{dist}(b_{ij}^1\xi^1 + b_{ij}^2\xi^2 + b_{ij}^3\xi^3, o_k)}{\partial t}\right|.$$

The above relationship holds at every point, so we have:

$$\begin{aligned}
L_1^{ij} &= \max \left|\frac{\partial \text{dist}(b_{ij}(t,\theta),o_k)}{\partial t}\right| \\
&\le \max \left|\frac{\partial \text{dist}(b_{ij}(t,\theta),o_k)}{\partial b_{ij}^1\xi^1 + b_{ij}^2\xi^2 + b_{ij}^3\xi^3} \frac{\partial b_{ij}^1\xi^1 + b_{ij}^2\xi^2 + b_{ij}^3\xi^3}{\partial \Theta(t,\theta)} \frac{\partial \Theta(t,\theta)}{\partial t}\right| \\
&\le \max \sum_{m=1}^3 \left|\frac{\partial b_{ij}^m(t,\theta)}{\partial \Theta(t,\theta)}\right|_{2,1} \xi^m \le \max_{m=1,\cdots,3} \left|\frac{\partial b_{ij}^m(t,\theta)}{\partial \Theta(t,\theta)}\right|_{2,1},
\end{aligned}$$

where the last inequality is due to the fact that $\xi^{1,2,3}$ form a convex combination. In other words, the Lipschitz constant of a moving triangle is the maximal Lipschitz constant over its three vertices. And the case is identical for a moving edge.

It remains to evaluate the upper bound of the $2,1$-norm of the Jacobian matrix for a moving point b_{ij}. We can derive this bound from the forward kinematic function. For simplicity, we assume a robot arm with only hinge joints as illustrated in the inset. We use Θ_k to denote the angle of the kth hinge joint. If b_{ij} lies on the Kth link, then only $\Theta_{1,\cdots,K}$ can affect the position of b_{ij}. We assume the kth link has length l_k, then the maximal influence of Θ_k on b_{ij} happens when all the $k,\cdots,K$th links are straight, so that:

$$\left|\frac{\partial b_{ij}}{\partial \Theta_k}\right| \le \sum_{m=1}^k l_m \implies \left|\frac{\partial b_{ij}}{\partial \Theta}\right|_{2,1} \le \sum_{k=1}^K \sum_{m=k}^K l_m.$$

B. High-Order Polynomial Trajectory Parameterization

Our L_1^{ij} formulation relies on the boundedness of $\partial \Theta(t,\theta)/\partial t$. And articulated robots can have joint limits

which must be satisfied at any $t \in [0,T]$. To these ends, we use high-order composite Bézier curves to parameterize the trajectory $\Theta(t,\theta)$ in the configuration space, so that $\Theta(t,\theta)$ is a high-order polynomial function. In this form, bounds on $\Theta(t,\theta)$ at an arbitrary t can be transformed into bounds on its control points [39]. We denote the lower- and upper-joint limits as $\underline{\Theta}$ and $\bar{\Theta}$, respectively. If we denote by M_k the matrix extracting the control points of Θ_k and M_{ik} the ith row of M_k, then the joint limit constraints can be conservatively enforced by the following log-barrier function:

$$\sum_i \sum_k \mathcal{P}(\bar{\Theta}_k - M_{ik}\Theta_k) + \mathcal{P}(-\underline{\Theta}_k + M_{ik}\Theta_k).$$

A similar approach can be used to bound $\partial \Theta_k(t,\theta)/\partial t$ to the range $[-1,1]$. We know that the gradient of a Bézier curves is another Bézier curves with a lower-order, so we can denote by M_k' the matrix extracting the control points of $\partial \Theta_k(t,\theta)/\partial t$ and M_{ik}' the ith row of M_k'. The boundedness of $\partial \Theta(t,\theta)/\partial t$ for any t can then be realized by adding the following log-barrier function:

$$\sum_i \sum_k \mathcal{P}(1 - M_{ik}'\Theta_k) + \mathcal{P}(1 + M_{ik}'\Theta_k).$$

Note that these constraints are strictly conservative. However, one can always use more control points in the Bézier curve composition to allow an arbitrarily long trajectory of complex motions.

C. Accelerated Computation of Barrier Functions

A naive method for computing the barrier function terms $\sum_{ijkl} \mathcal{P}_{ijkl}$ could be prohibitively costly, and we propose several acceleration techniques that is compatible with our theoretical analysis. Note first that our theoretical results assume the same L_1 for all b_{ij}, but the L_1^{ij} constant computed in Section VI-A is different for each b_{ij}. Instead of letting $L_1 = \max_{ij} L_1^{ij}$, we could use a different $\phi(x) = L_1^{ij}x/2 + L_2 x^\eta$ for each b_{ij}, leading to a loose safety condition and less subdivisions. Further, note that our potential function $\mathcal{P}$ is locally supported by design and we only need to compute $\mathcal{P}_{ijk}$ if the distance between b_{ij} and o_k is less than x_0. We propose to build a spatial-temporal, binary-tree-based bounding volume hierarchy (BVH) [40] for pruning unnecessary $\mathcal{P}_{ijk}$ terms, where each leaf node of our BVH indicates a unique tuple $< b_{ij}, T_0^l, T_1^l >$. Upon subdivision, a leaf node
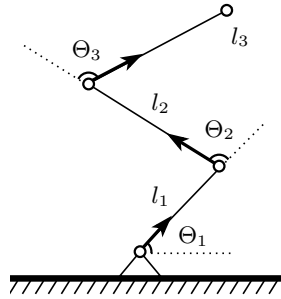
tuple $< b_{ij}, T_0^l, T_1^l >$ is replaced by an internal node with two children: $< b_{ij}, T_0^l, (T_0^l + T_1^l)/2 >$ and $< b_{ij}, (T_0^l + T_1^l)/2, T_1^l >$. The BVH can be checked against each obstacle o_k to quickly prune $< b_{ij}, o_k >$ pairs with distance larger than x_0.

D. Barrier Functions Between Convex Hulls

In our first version of algorithm, we assume all the geometries are discretized using triangular meshes. Although triangular meshes can represent arbitrary concave shapes, they requires a large number of elements leading to prohibitive overhead even using the acceleration techniques introduced in Section VI-C. A common technique to reduce the number of geometric primitives is by approximating each robot link and obstacle with a single convex hull [16], [41] or multiple convex hulls via a convex decomposition [42]. However, convex approximation is not immediately applicable in our approach because the distance function between convex hulls is not differentiable [14]. We follow [32] to resolve this problem by bulging each convex hull using curved surfaces, making them strictly convex with well-defined derivatives of the distance function. Finally, the L_1^{ij} constant of a convex hull is the maximal Lipschitz constant over all its vertices.

E. Handling Self-Collisions

Our theoretical results inherently apply to handle self-collisions. Indeed, for two articulated robot subsets b_{ij} and $b_{i'j'}$, we could transform b_{ij} into the reference frame of $b_{i'}^0$, in which $b_{i'j'}$ can be viewed as a static obstacle. In practice, however, it is more convenient to use the following alternative definition of $\phi(x)$ within the safety check:

$$\phi(x) = (L_1^{ij} + L_1^{i'j'})x/2 + L_2 x^\eta.$$

Further, note that the subdivision status of b_{ij} and $b_{i'j'}$ can be different. For example, b_{ij} can have a subdivision interval $[T_0^l, T_1^l]$, while $b_{i'j'}$ has an overlapping interval $[T_0^{l'}, T_1^{l'}]$ such that $[T_0^l, T_1^l) \cap [T_0^{l'}, T_1^{l'}) \neq \varnothing$, but $[T_0^l, T_1^l] \neq [T_0^{l'}, T_1^{l'}]$. Since we use the midpoint constraint as the representative of the interval, there is no well-defined midpoint for such inconsistent interval pairs. To tackle this issue, we note that by the midpoint subdivision rule, we have either $[T_0^l, T_1^l] \subset [T_0^{l'}, T_1^{l'}]$ or $[T_0^{l'}, T_1^{l'}] \subset [T_0^l, T_1^l]$. As a result, we could recursively subdivide the larger interval until the two intervals are identical.

VII. EVALUATION

We implement our method using C++ and evaluate the performance on a single desktop machine with one 32-core AMD 3970x CPU. We make full use of the CPU cores to parallelize the BVH collision check, energy function, and derivative computations. For all our experiments, we use $x_0 = 10^{-3}$, $L_2 = 10^{-4}$, $\eta = 1/7$, $\mu = 10^{-2}$. The trajectory is parameterized in configuration space using a 5th-order composite Bézier curve with 5 segments over a horizon of $T = 5$s. We use four computational benchmarks discussed below.
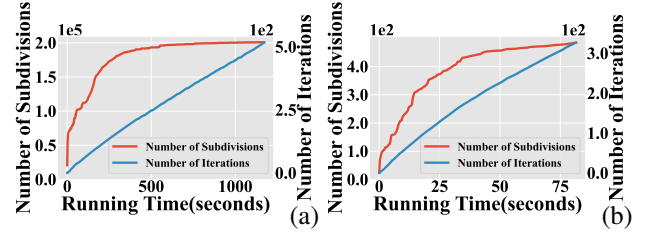

Fig. 4: The number of subdivisions and iterations plotted against the computational time for our first benchmark using triangular mesh (a) and convex hull (b) representations.

A. Benchmark Problems

Our first benchmark (Figure 3a) involves two LBR iiwa robot arms simultaneously reaching several target points in a shared workspace. To this end, our objective function involves a distance measure between the robot end-effectors and the target points, as well as a Laplacian trajectory smoothness metric as in [29]. The convergence history as well as the number of subdivisions is plotted in Figure 4 for both versions of geometric representations: triangular mesh and convex hull. Our method using triangular meshes is much slower than that using convex hulls, due to the fine geometric details leading to a large number of triangle-triangle pairs. Our method with the convex hull representation converges after 485 subdivisions, 89 iterations, and 2.01 minutes of computation.

Our second benchmark (Figure 3b with successful points in green and unsuccessful points in red) involves a single LBR iiwa robot arm interacting with a tree-like obstacle with thin geometric objects. Such obstacles can lead to ill-defined gradients for infeasible discretization methods or even tunnel through robot links [1], while our method can readily handle such ill-shaped obstacles. We sample a grid of target positions for the end-effector to reach and run our algorithm for each position. Our method can successfully reach 16/56 positions. We further conduct an exhaustive search for each unsuccessful point. Specifically, if an unsuccessful point is neighboring a successful point, we optimize an additional trajectory for the end-effector to connect the two points. Such connection is performed until no new points can be reached. In this way, our method can successfully reach 39/56 positions. On average, to reach each target point, our method with the convex hull representation converges after 416 subdivisions, 246 iterations, and 0.31 minutes of computation.
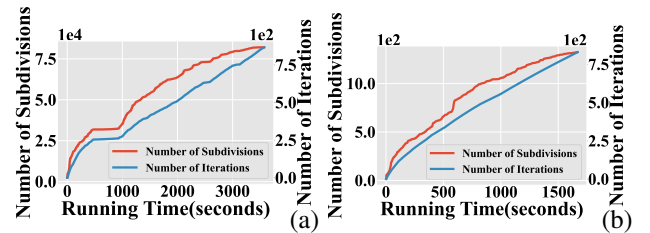

Fig. 5: The number of subdivisions and iterations plotted against the computational time for our third benchmark using triangular mesh (a) and convex hull (b) representatoins.

Our third benchmark (Figure 3c) involves a swarm of six

UAVs navigating across each other through another swarm of spherical obstacles. A UAV can be modeled as a free-flying rigid body with 6 degrees of freedom. Unlike prior work [30] that searches for only the translations, we can optimize both the translation and rotation. We have experimented with both geometric representations and the convergence history of this example is plotted Figure 5. Our method with the convex hull representation converges after 777 subdivisions, 638 iterations, and 44.25 minutes of computation. In Figure 6, we plot the
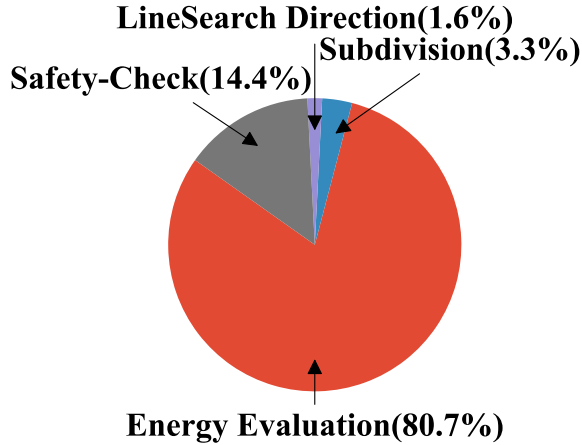

Fig. 6: Over an optimization, we plot the fraction of computation on each component. Our major bottleneck lies in the energy evaluation and safety check, taking 80.7% and 14.4% of the computation, respectively.

fraction of computation for each component of our method. Our major bottleneck lies in the energy evaluation, i.e. computing $\mathcal{E}(\theta)$ and its derivatives. Note that we use either triangular mesh or convex hull as our geometric representation. In the former case, the number of $\mathcal{P}_{ijkl}$ terms is large, leading to a major computational burden. In the later case, the number of $\mathcal{P}_{ijkl}$ terms is much smaller, but each evaluation of $\mathcal{P}_{ijkl}$ involves the non-trivial computation of the shortest distance between convex hulls.

Our final benchmark (Figure 3d) plans for an armed mobile robot to reach a grid of locations on a book-shelf. We use convex decomposition to represent both the robot links and the book-shelf as convex hulls. Starting from a faraway initial guess, our method can guide the robot to reach 88/114 target positions, achieving a success rate of 77.19%. On average over each target point, our method with the convex hull representation converges after 874 subdivision, 402 iterations, and 1.77 minutes of computation.

B. Comparisons with Exchange Method

For fair comparisons, we have re-implemented the exchange method [14] in our framework. The exchange method samples the robot and obstacle surfaces into a point cloud. During each iteration, the deepest penetration point between each pair of convex objects is detected at sampled locations and inserted into the index set. Unlike the original work where a signed distance field is used to find the penetration depth, we use

the exact point-to-mesh distance computation that is more accurate. We also adopt the same branch-and-bound technique as [14] to quickly prune points with insufficient penetration depth and we set the maximal time-resolution of penetration detection to be $\epsilon = 10^{-3}$. After the index set is updated, an NLP is formulated and solved using the IPOPT software package [43] to remove penetrations.
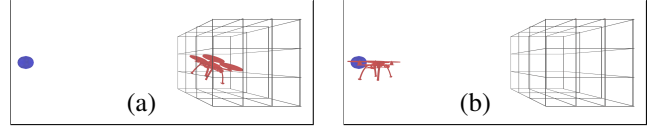

Fig. 7: A UAV is trapped inside a cage but trying to fly outside to the blue target point. We show final location of the UAV computed by our discretization method (a) and the exchange method (b).

First, we notice the exchange method does not have the feasibility guarantee, i.e., might not converge to a feasible solution even from a feasible initial guess. We demonstrate this phenomena with a toy example illustrated in Figure 7, where a UAV is trapped in a cage consisting of a row of metal bars. The UAV is trying to fly to the target point outside. Our method would get the UAV close to the target point but still trapped inside the cage, while the exchange method will erroneously get the UAV outside the cage however small ϵ is. This seemingly surprising result is due to the fact that the exchange method ultimately detects penetrations at discrete time instances with a resolution of ϵ. However, the optimizer is allowed to arbitrarily accelerate the UAV to a point where it can fly out of the cage within ϵ, and the collision constraint will be missed.

Next, we run the two algorithms on the first and third benchmarks above, which involve only a single target position for the robots. (The other two benchmarks involve a grid of target positions making it too costly to compute using the exchange method.) The exchange method succeeds in both benchmarks.On the first benchmark, the exchange method takes 33.09 minutes to finish the computation after 123 index set updates and NLP solves, while our method only takes 5.47 minutes. Similarly, on the third benchmark, the exchange method takes 699.23 minutes to finish the computation after 1804 index set updates and NLP solves, while our method only takes 30.02 minutes. The performance advantage of our method is for two reasons: First, our method does not require the collision to be detected at the finest resolution ($\epsilon = 10^{-3}$ in the exchange method). Instead, we only need a subdivision that is sufficient to find descendent directions. Second, our method does not require the NLP to be solved exactly after each update of the energy function. We only run one iteration of Newton's method per round of subdivision. Notice that the original method [14] also proposed to partially solve the NLP using a small number of iterations. However, this requires heuristic tuning of iteration numbers without theoretical guarantee of overall convergence.

VIII. Conclusion

We propose the first provably robust algorithm for collision-free trajectory generation of articulated robots. We formulate the underlying SIP problem and solve it using a novel feasible discretization method. Our method divides the temporal domain into discrete intervals and chooses one representative constraint for each interval, reducing the SIP to an NLP. We further propose a conservative motion bound that ensures the original SIP constraint is satisfied. Finally, we establish theoretical convergence guarantee and propose practical implementations for articulated robots. Our results show that our method can generate long-horizon trajectories for industrial robot arms within a couple minutes of computation.

Our method opens doors to several directions of future work. First, our method does not account for the dynamics of the robot. Generating collision-free dynamic trajectories can be achieved by introducing additional equality constraints at sampled time instances. But enforcing infinite dynamic constraints for each time instance is challenging because our method can only handle inequality constraints. Second, the linear motion bound Lemma IV.2 is too conservative and high-order Taylor models [27] can potentially reduce the number of subdivisions and improve the computational speed.

References

[1] J. Schulman, Y. Duan, J. Ho, A. Lee, I. Awwal, H. Bradlow, J. Pan, S. Patil, K. Goldberg, and P. Abbeel, "Motion planning with sequential convex optimization and convex collision checking," *The International Journal of Robotics Research*, vol. 33, no. 9, pp. 1251–1270, 2014.

[2] K. J. Kyriakopoulos and G. N. Saridis, "Minimum jerk path generation," in *Proceedings. 1988 IEEE international conference on robotics and automation*, IEEE, 1988, pp. 364–369.

[3] C. Hansen, J. Öltjen, D. Meike, and T. Ortmaier, "Enhanced approach for energy-efficient trajectory generation of industrial robots," in *2012 IEEE International Conference on Automation Science and Engineering (CASE)*, IEEE, 2012, pp. 1–7.

[4] T. Kunz and M. Stilman, "Time-optimal trajectory generation for path following with bounded acceleration and velocity," *Robotics: Science and Systems VIII*, pp. 1–8, 2012.

[5] S. M. LaValle *et al.*, "Rapidly-exploring random trees: A new tool for path planning," 1998.

[6] S. Karaman and E. Frazzoli, "Sampling-based algorithms for optimal motion planning," *The International Journal of Robotics Research*, vol. 30, no. 7, pp. 846–894, 2011.

[7] J. Pan, S. Chitta, and D. Manocha, "Fcl: A general purpose library for collision and proximity queries," in *2012 IEEE International Conference on Robotics and Automation*, IEEE, 2012, pp. 3859–3866.

[8] B. V. Mirtich, *Impulse-based dynamic simulation of rigid body systems*. University of California, Berkeley, 1996.

[9] S. Redon, A. Kheddar, and S. Coquillart, "Fast continuous collision detection between rigid bodies," in *Computer graphics forum*, Wiley Online Library, vol. 21, 2002, pp. 279–287.

[10] Y.-K. Choi, W. Wang, Y. Liu, and M.-S. Kim, "Continuous collision detection for two moving elliptic disks," *IEEE Transactions on Robotics*, vol. 22, no. 2, pp. 213–224, 2006.

[11] Y.-K. Choi, J.-W. Chang, W. Wang, M.-S. Kim, and G. Elber, "Continuous collision detection for ellipsoids," *IEEE Transactions on visualization and Computer Graphics*, vol. 15, no. 2, pp. 311–325, 2008.

[12] T. Brochu, E. Edwards, and R. Bridson, "Efficient geometrically exact continuous collision detection," *ACM Transactions on Graphics (TOG)*, vol. 31, no. 4, pp. 1–7, 2012.

[13] J. Schulman, J. Ho, A. X. Lee, I. Awwal, H. Bradlow, and P. Abbeel, "Finding locally optimal, collision-free trajectories with sequential convex optimization.," in *Robotics: science and systems*, Citeseer, vol. 9, 2013, pp. 1–10.

[14] K. Hauser, "Semi-infinite programming for trajectory optimization with non-convex obstacles," *The International Journal of Robotics Research*, vol. 40, no. 10-11, pp. 1106–1122, 2021.

[15] M. López and G. Still, "Semi-infinite programming," *European journal of operational research*, vol. 180, no. 2, pp. 491–518, 2007.

[16] A. Amice, H. Dai, P. Werner, A. Zhang, and R. Tedrake, "Finding and optimizing certified, collision-free regions in configuration space for robot manipulators," *arXiv preprint arXiv:2205.03690*, 2022.

[17] A. Majumdar, A. A. Ahmadi, and R. Tedrake, "Control design along trajectories with sums of squares programming," in *2013 IEEE International Conference on Robotics and Automation*, IEEE, 2013, pp. 4054–4061.

[18] A. Clark, "Verification and synthesis of control barrier functions," in *2021 60th IEEE Conference on Decision and Control (CDC)*, IEEE, 2021, pp. 6105–6112.

[19] A. Majumdar and R. Tedrake, "Funnel libraries for real-time robust feedback motion planning," *The International Journal of Robotics Research*, vol. 36, no. 8, pp. 947–982, 2017.

[20] M. Zhang and K. Hauser, "Semi-infinite programming with complementarity constraints for pose optimization with pervasive contact," in *2021 IEEE International Conference on Robotics and Automation (ICRA)*, IEEE, 2021, pp. 6329–6335.

[21] L. Vandenberghe and S. Boyd, "Connections between semi-infinite and semidefinite programming," in *Semi-infinite programming*, Springer, 1998, pp. 277–294.

[22] P. A. Parrilo, *Structured semidefinite programs and semialgebraic geometry methods in robustness and optimization*. California Institute of Technology, 2000.

[23] T. Pietrzykowski, "An exact potential method for constrained maxima," *SIAM Journal on numerical analysis*, vol. 6, no. 2, pp. 299–304, 1969.

[24] A. R. Conn and N. I. Gould, "An exact penalty function for semi-infinite programming," *Mathematical Programming*, vol. 37, no. 1, pp. 19–40, 1987.

[25] U. Borrmann, L. Wang, A. D. Ames, and M. Egerstedt, "Control barrier certificates for safe swarm behavior," *IFAC-PapersOnLine*, vol. 48, no. 27, pp. 68–73, 2015.

[26] A. D. Ames, S. Coogan, M. Egerstedt, G. Notomista, K. Sreenath, and P. Tabuada, "Control barrier functions: Theory and applications," in *2019 18th European control conference (ECC)*, IEEE, 2019, pp. 3420–3431.

[27] X. Zhang, S. Redon, M. Lee, and Y. J. Kim, "Continuous collision detection for articulated models using taylor models and temporal culling," *ACM Trans. Graph.*, vol. 26, no. 3, 15–es, Jul. 2007.

[28] N. Ratliff, M. Zucker, J. A. Bagnell, and S. Srinivasa, "Chomp: Gradient optimization techniques for efficient motion planning," in *2009 IEEE International Conference on Robotics and Automation*, IEEE, 2009, pp. 489–494.

[29] C. Park, J. Pan, and D. Manocha, "Itomp: Incremental trajectory optimization for real-time replanning in dynamic environments," in *Twenty-Second International Conference on Automated Planning and Scheduling*, 2012.

[30] H. Oleynikova, M. Burri, Z. Taylor, J. Nieto, R. Siegwart, and E. Galceran, "Continuous-time trajectory optimization for online uav replanning," in *2016 IEEE/RSJ International Conference on Intelligent Robots and Systems (IROS)*, IEEE, 2016, pp. 5332–5339.

[31] R. Deits and R. Tedrake, "Efficient mixed-integer planning for uavs in cluttered environments," in *2015 IEEE international conference on robotics and automation (ICRA)*, IEEE, 2015, pp. 42–49.

[32] A. Escande, S. Miossec, M. Benallegue, and A. Kheddar, "A strictly convex hull for computing proximity distances with continuous gradients," *IEEE Transactions on Robotics*, vol. 30, no. 3, pp. 666–678, 2014.

[33] D. Harmon, E. Vouga, B. Smith, R. Tamstorf, and E. Grinspun, "Asynchronous contact mechanics," in *ACM SIGGRAPH 2009 Papers*, ser. SIGGRAPH '09, New York, NY, USA: Association for Computing Machinery, 2009.

[34] P. Armand, J. C. Gilbert, and S. Jan-Jégou, "A Feasible BFGS Interior Point Algorithm for Solving Strongly Convex Minimization Problems," INRIA, Research Report RR-3500, 1998.

[35] U. Schättler, "An interior-point method for semi-infinite programming problems," *Annals of Operations Research*, vol. 62, no. 1, pp. 277–301, 1996.

[36] D. P. Bertsekas, "Nonlinear programming," *Journal of the Operational Research Society*, vol. 48, no. 3, pp. 334–334, 1997.

[37] M. Tang, D. Manocha, and R. Tong, "Fast continuous collision detection using deforming non-penetration filters," in *I3D '10: Proceedings of the 2010 ACM SIGGRAPH symposium on Interactive 3D Graphics and Games*, New York, NY, USA: ACM, 2010, pp. 7–13.

[38] S. Osher and R. P. Fedkiw, *Level set methods and dynamic implicit surfaces*. Springer New York, 2005, vol. 1.

[39] E. V. Shikin and A. I. Plis, *Handbook on Splines for the User*. CRC press, 1995.

[40] Y. Gu, Y. He, K. Fatahalian, and G. Blelloch, "Efficient bvh construction via approximate agglomerative clustering," in *Proceedings of the 5th High-Performance Graphics Conference*, 2013, pp. 81–88.

[41] H. Dai, A. Majumdar, and R. Tedrake, "Synthesis and optimization of force closure grasps via sequential semidefinite programming," in *Robotics Research*, Springer, 2018, pp. 285–305.

[42] J.-M. Lien and N. M. Amato, "Approximate convex decomposition of polygons," in *Proceedings of the twentieth annual symposium on Computational geometry*, 2004, pp. 17–26.

[43] L. T. Biegler and V. M. Zavala, "Large-scale nonlinear programming using ipopt: An integrating framework for enterprise-wide dynamic optimization," *Computers & Chemical Engineering*, vol. 33, no. 3, pp. 575–582, 2009.

IX. FINITE TERMINATION OF ALGORITHM 1

We show that Algorithm 1 would terminate after finitely many iterations. We will omit the parameter of a function whenever there can be no confusion. Our main idea is to compare the following two terms:

$$\tilde{\mathcal{P}} \triangleq \sum_{ijkl}(T_1^l - T_0^l)\mathcal{P}_{ijkl} \quad \bar{\mathcal{P}} \triangleq \sum_{ijkl}\int_{T_0^l}^{T_1^l}\mathcal{P}_{ijk}(t)dt,$$

where we use a shorthand notation $\tilde{\mathcal{P}}$ for the penalty function part of Equation (8). Conceptually, $\tilde{\mathcal{P}}$ approximates $\bar{\mathcal{P}}$ in the sense of Riemann sum and the approximation error would reduce as more subdivisions are performed. However, the approximation error will not approach zero because our subdivision is adaptive. Therefore, we need a new tool to analyze the difference between $\tilde{\mathcal{P}}$ and $\bar{\mathcal{P}}$. To this end, we introduce the following hybrid penalty function with a variable ϵ_2 controlling the level of hybridization:

$$\hat{\mathcal{P}}(\epsilon_2) = \sum_{ijkl}\begin{cases}(T_1^l - T_0^l)\mathcal{P}_{ijkl} & T_1^l - T_0^l \geq \epsilon_2 \\ \int_{T_0^l}^{T_1^l}\mathcal{P}_{ijk}(t)dt & T_1^l - T_0^l < \epsilon_2,\end{cases}$$

where we use the integral form when a temporal interval is shorter than ϵ_2, while use the surrogate constraint otherwise. An important property of $\hat{\mathcal{P}}(\epsilon_2)$ is that it is invariant to subdivision after finitely many iterations:

Lemma IX.1. *Given fixed ϵ_2, and after finitely many times of subdivision, $\hat{\mathcal{P}}(\epsilon_2)$ becomes invariant to further subdivision.*

Proof. Since each subdivision would reduce a time interval by a factor of $1/2$, it takes finitely many subdivisions to reduce a time interval to satisfy: $T_1^l - T_0^l < \epsilon_2$. Therefore, after finitely many subdivision operators, a time interval must satisfy one of two cases: (Case I) No more subdivisions are applied to it, making it invariant to further subdivisions; (Case II) The time

interval $T_1^l - T_0^l < \epsilon_2$ and infinitely many subdivisions will be applied, but the integral is invariant to subdivision. $\square$

Next, we show that the difference between $\hat{\mathcal{P}}$ and $\tilde{\mathcal{P}}$ is controllable via ϵ_2. The following result bound their differences:

Lemma IX.2. *Taking Assumption III.1, IV.1, IV.3, and assuming θ is generated by some iteration of Algorithm 1, we have:*

$$\left|\hat{\mathcal{P}}(\epsilon_2) - \tilde{\mathcal{P}}\right| = \boldsymbol{O}(\epsilon_2^{1-5\eta}),$$

for arbitrarily small fixed ϵ_2.

Proof. We use the shorthand notation $\sum_{ijkl}^{\Delta T < \epsilon_2}$ to denote a summation over intervals $T_1^l - T_0^l < \epsilon_2$, and the following abbreviations are used:

$$d_t \triangleq \text{dist}\left(b_{ij}\left(t, \theta\right), o_k\right) - d_0$$
$$d_m \triangleq \text{dist}\left(b_{ij}\left(\frac{T_0^l + T_1^l}{2}, \theta\right), o_k\right) - d_0.$$

Since θ is generated by line search, we have θ passes the safety check, leading to the following result:

$$\left|\mathcal{P}_{ijk}(t) - \mathcal{P}_{ijkl}\right| = \left|\int_{d_t}^{d_m} \frac{\partial \mathcal{P}(x)}{\partial x} dx\right|$$
$$\leq \left|\frac{\partial \mathcal{P}(x)}{\partial x}\right|_{L_2(T_1^l - T_0^l)^\eta} |d_m - d_t|$$
$$\leq L_1 \left|\frac{\partial \mathcal{P}(x)}{\partial x}\right|_{L_2(T_1^l - T_0^l)^\eta} \left|t - \frac{T_0^l + T_1^l}{2}\right|.$$

The second inequality above is due to the safety check condition and monotonicity of $\mathcal{P}, |\nabla_x \mathcal{P}|$. The third inequality above is due to Lemma IV.2. The result in our lemma is derived immediately as follows:

$$\left|\hat{\mathcal{P}}(\epsilon_2) - \tilde{\mathcal{P}}\right| \leq \sum_{ijkl}^{\Delta T < \epsilon_2} \int_{T_0^l}^{T_1^l} \left|\mathcal{P}_{ijk}(t) - \mathcal{P}_{ijkl}\right| dt$$
$$\leq \sum_{ijkl}^{\Delta T < \epsilon_2} L_1 \left|\frac{\partial \mathcal{P}(x)}{\partial x}\right|_{L_2(T_1^l - T_0^l)^\eta} \left|\int_{T_0^l}^{T_1^l} \left|t - \frac{T_0^l + T_1^l}{2}\right| dt\right.$$
$$\leq \sum_{ijkl}^{\Delta T < \epsilon_2} L_1 \frac{(T_1^l - T_0^l)^2}{4} \left|\frac{\partial \mathcal{P}(x)}{\partial x}\right|_{L_2(T_1^l - T_0^l)^\eta}$$
$$\leq \sum_{ijkl} \frac{T + \epsilon_2}{\epsilon_2} L_1 \frac{(T_1^l - T_0^l)^2}{4} \left|\frac{\partial \mathcal{P}(x)}{\partial x}\right|_{L_2(T_1^l - T_0^l)^\eta}$$
$$= \sum_{ijkl} \frac{T + \epsilon_2}{\epsilon_2} L_1 (T_1^l - T_0^l) \Gamma(T_1^l - T_0^l)$$
$$\Gamma(T_1^l - T_0^l) \triangleq \frac{T_1^l - T_0^l}{4} \left|\frac{\partial \mathcal{P}(x)}{\partial x}\right|_{L_2(T_1^l - T_0^l)^\eta}.$$

The last inequality above is by the assumption that the entire temporal domain $[0, T]$ is subdivided into intervals of length smaller than ϵ_2. It can be shown by direct verification that by choosing $\eta < 1/5$, $\Gamma(T_1^l - T_0^l) = \boldsymbol{O}(\epsilon_2^{1-5\eta})$ as $T_1^l - T_0^l \to 0$ and the lemma is proved. $\square$

In a similar fashion to Lemma IX.2, we can bound the difference in gradient:

Lemma IX.3. *Taking Assumption III.1, IV.1, IV.3, and assuming θ is generated by some iteration of Algorithm 1, we have:*

$$\left\|\nabla_\theta \hat{\mathcal{P}}(\epsilon_2) - \nabla_\theta \tilde{\mathcal{P}}\right\| = \boldsymbol{O}(\epsilon_2^{1-6\eta}),$$

for arbitrarily small fixed ϵ_2.

Proof. Again, we use the shorthand notations: $\sum_{ijkl}^{\Delta T < \epsilon_2}$, d_t, and d_m. We begin by bounding the error of the integrand:

$$\left\|\nabla_\theta \mathcal{P}_{ijk}(t) - \nabla_\theta \mathcal{P}_{ijkl}\right\|$$
$$= \left\|\frac{\partial \mathcal{P}(d_t)}{\partial d_t} \nabla_\theta d_t - \frac{\partial \mathcal{P}(d_m)}{\partial d_m} \nabla_\theta d_m\right\|$$
$$\leq \left|\frac{\partial \mathcal{P}(d_t)}{\partial d_t}\right| \|\nabla_\theta d_t - \nabla_\theta d_m\| + \left|\frac{\partial \mathcal{P}(d_t)}{\partial d_t} - \frac{\partial \mathcal{P}(d_m)}{\partial d_m}\right| \|\nabla_\theta d_m\|,$$

which is due to triangle inequality. There are two terms in the last equation to be bounded. To bound the first term, we use a similar argument as Lemma IV.2. Under Assumption IV.1, there must exist some constant L_3 such that:

$$\|\nabla_\theta d_t - \nabla_\theta d_m\| \leq L_3 \left|t - \frac{T_0^l + T_1^l}{2}\right|.$$

Since θ passes the safety check, we further have:

$$\left|\frac{\partial \mathcal{P}(d_t)}{\partial d_t}\right| \|\nabla_\theta d_t - \nabla_\theta d_m\| \leq L_3 \left|\frac{\partial \mathcal{P}(x)}{\partial x}\right|_{L_2(T_1^l - T_0^l)^\eta} \left|t - \frac{T_0^l + T_1^l}{2}\right|.$$

To bound the second term, we note that $\|\nabla_\theta d_m\| \leq L_4$ for some L_4 because its domain is bounded. By the mean value theorem, we have:

$$\left|\frac{\partial \mathcal{P}(d_t)}{\partial d_t} - \frac{\partial \mathcal{P}(d_m)}{\partial d_m}\right| \|\nabla_\theta d_m\| \leq L_4 \left|\int_{d_t}^{d_m} \frac{\partial^2 \mathcal{P}(x)}{\partial x^2} dx\right|$$
$$\leq L_4 \left|\frac{\partial^2 \mathcal{P}(x)}{\partial x^2}\right|_{L_2(T_1^l - T_0^l)^\eta} \left|t - \frac{T_0^l + T_1^l}{2}\right|,$$

where we have used the safety check condition and monotonicity of $|\nabla_x^2 \mathcal{P}|$. Putting everything together, we establish the result in our lemma as follows:

$$\left\|\nabla_\theta \hat{\mathcal{P}}(\epsilon_2) - \nabla_\theta \tilde{\mathcal{P}}\right\| \leq \sum_{ijkl}^{\Delta T < \epsilon_2}$$
$$L_3(T_1^l - T_0^l)\Gamma(T_1^l - T_0^l) + L_4(T_1^l - T_0^l)\Gamma'(T_1^l - T_0^l)$$
$$\Gamma'(T_1^l - T_0^l) \triangleq \frac{T_1^l - T_0^l}{4} \left|\frac{\partial^2 \mathcal{P}(x)}{\partial x^2}\right|_{L_2(T_1^l - T_0^l)^\eta}.$$

It can be shown that Γ' is the dominating term and, by direct verification, we have $\Gamma'(T_1^l - T_0^l) = \boldsymbol{O}(\epsilon_2^{1-6\eta})$ as $T_1^l - T_0^l \to 0$, which proves our lemma. $\square$

A. Finite Termination of Algorithm 3

We are now ready to show the finite termination of the line search Algorithm 3. If Algorithm 3 does not terminate, it must make infinitely many calls to the subdivision function. Otherwise, suppose only finitely many calls to the subdivision

is used, Algorithm 3 reduces to a standard line search for NLP after the last call, which is guaranteed to succeed. However, we show that using infinitely many subdivisions will contradict the finiteness of $\mathcal{E}(\theta)$.

Lemma IX.4. *Taking Assumption III.1, IV.1, IV.3, if Algorithm 3 makes infinitely many calls to subdivision, then θ is unsafe.*

Proof. Suppose Algorithm 3 is trying to update θ to $\theta' = \theta + d\alpha$. Such update must fail because only finitely many subdivisions are needed otherwise. Further, there must be some interval $[T_0^l, T_1^l]$ that requires infinitely many subdivisions. As a result, given any fixed ϵ_3 and ϵ_4, there must be some unsafe interval $[\bar{T}_0^l, \bar{T}_1^l] \subset [T_0^l, T_1^l]$ such that:

$$\bar{T}_1^l - \bar{T}_0^l \leq \epsilon_3 \quad \alpha \leq \epsilon_4.$$

We use the following shorthand notation:

$$\bar{\mathcal{P}}_{ijkl} \triangleq \mathcal{P}\left(\text{dist}\left(b_{ij}\left(\frac{\bar{T}_0^l + \bar{T}_1^l}{2}, \theta\right), o_k\right) - d_0\right)$$

$$\mathcal{P}'_{ijkl} \triangleq \mathcal{P}\left(\text{dist}\left(b_{ij}\left(\frac{\bar{T}_0^l + \bar{T}_1^l}{2}, \theta'\right), o_k\right) - d_0\right)$$

$$d_m \triangleq \text{dist}\left(b_{ij}\left(\frac{\bar{T}_0^l + \bar{T}_1^l}{2}, \theta\right), o_k\right) - d_0$$

$$d'_m \triangleq \text{dist}\left(b_{ij}\left(\frac{\bar{T}_0^l + \bar{T}_1^l}{2}, \theta'\right), o_k\right) - d_0.$$

Since the interval is unsafe, we have:

$$\mathcal{P}'_{ijkl} \geq \mathcal{P}(\psi(\bar{T}_1^l - \bar{T}_0^l)).$$

Finally, we can bound the difference between penalty functions evaluated at θ and that at θ' using mean value theorem:

$$\left|\mathcal{P}'_{ijkl} - \bar{\mathcal{P}}_{ijkl}\right| = \left|\int_{d_m}^{d'_m} \frac{\partial \mathcal{P}(x)}{\partial x} dx\right|$$

$$\leq \max_{x \in [d_m, d'_m]} \left|\frac{\partial \mathcal{P}(x)}{\partial x}\right| |d_m - d'_m|$$

$$\leq L_4 \max_{x \in [d_m - L_4\|d\|\epsilon_4, d_m + L_4\|d\|\epsilon_4]} \left|\frac{\partial \mathcal{P}(x)}{\partial x}\right| \|d\| \epsilon_4.$$

The above result implies that the difference between the two penalty functions is controllable via ϵ_4. Since both ϵ_3 and ϵ_4 are arbitrary and independent, we can choose small ϵ_4 such that:

$$\bar{\mathcal{P}}_{ijkl} = \Theta(\mathcal{P}'_{ijkl}) \geq \Theta(\mathcal{P}(\psi(\bar{T}_1^l - \bar{T}_0^l))) \geq \Theta(\mathcal{P}(\psi(\epsilon_3))).$$

But for θ to be safe, we need:

$$\bar{\mathcal{P}}_{ijkl} \leq \mathcal{P}(L_2(T_1^l - T_0^l)^\eta),$$

so θ cannot be safe. □

Corollary IX.5. *Algorithm 3 makes finitely many calls to subdivision, i.e., terminate finitely.*

Proof. Algorithm 1 requires the initial θ to be feasible, so the initial θ is safe. Each iteration of Algorithm 1 generates feasible iterations by Theorem V.1. If infinitely many subdivisions are used, then Lemma IX.4 implies that some θ is unsafe, which is a contradiction. □

B. Finite Termination of Algorithm 1

After showing the finite termination of Lemma IX.4, we move on to show the finite termination of main Algorithm 1. Our main idea is to compare $\tilde{\mathcal{P}}$ and $\hat{\mathcal{P}}$ and bound their difference. We first show that: $\hat{\mathcal{P}}$ is unbounded if infinite number of subdivisions are needed:

Lemma IX.6. *Taking Assumption III.1, IV.1, IV.3, for any fixed ϵ_5, if Algorithm 3 makes infinitely many calls to subdivision, then either $\hat{\mathcal{P}}(\epsilon_5)$ is unbounded or θ is unsafe.*

Proof. Following the same argument as Lemma IX.4, there must be unsafe interval $[\bar{T}_0^l, \bar{T}_1^l] \subset [T_0^l, T_1^l]$ with $\mathcal{P}_{ijkl} = \Theta(\mathcal{P}'_{ijkl}) \geq \Theta(\mathcal{P}(\psi(\epsilon_3)))$ for any fixed ϵ_3. Since the domain is compact, there must be some $t \in [T_0^l, T_1^l]$ such that $\mathcal{P}_{ijk}(t) = \infty$. There are two cases for the interval $[T_0^l, T_1^l]$: (Case I) If $T_1^l - T_0^l < \epsilon_5$, then $\hat{\mathcal{P}}(\epsilon_5)$ is using the integral formula for the interval and $\mathcal{P}$ is unbounded by Lemma IV.4. (Case II) If $T_1^l - T_0^l \geq \epsilon_5$, then θ is unsafe by Lemma IX.4. □

Our final proof uses the Wolfe's condition to derive a contradiction if infinite number of subdivisions are needed. Specifically, we will show that the search direction is descendent if $\tilde{P}$ is replaced by $\hat{P}$ for some small ϵ_2. The following argument assumes $d = d^{(1)}$ and the case with $d = d^{(2)}$ follows an almost identical argument.

Proof of Theorem V.2. Suppose otherwise, we have $\|d\|_\infty \geq \epsilon_d$ because the algorithm terminates immediately otherwise. Due to the equivalence of metrics, we have $\|d\| \geq \epsilon_6$ for some ϵ_6. We introduce the following shorthand notation:

$$\hat{\mathcal{E}}(\theta, \epsilon_2) = \mathcal{O}(\theta) + \mu \hat{\mathcal{P}}(\epsilon_2).$$

We consider an iteration of Algorithm 1 that updates from θ to θ'. Since the first Wolfe's condition holds, we have:

$$\mathcal{E}(\theta') \leq \mathcal{E}(\theta) - c\|\nabla_\theta \mathcal{E}(\theta)\|^2 \alpha \leq \mathcal{E}(\theta) - c\|\nabla_\theta \mathcal{E}(\theta)\|\alpha\epsilon_6.$$

The corresponding change in $\hat{\mathcal{E}}(\theta, \epsilon_2)$ can be bounded as follows:

$$\hat{\mathcal{E}}(\theta', \epsilon_2) = \hat{\mathcal{E}}(\theta, \epsilon_2) + \int_\theta^{\theta'} \left\langle \nabla_\theta \hat{\mathcal{E}}(\theta, \epsilon_2), d\theta \right\rangle$$

$$\leq \hat{\mathcal{E}}(\theta, \epsilon_2) + \int_\theta^{\theta'} \left\langle \nabla_\theta \hat{\mathcal{E}}(\theta, \epsilon_2) - \nabla_\theta \mathcal{E}(\theta) + \nabla_\theta \mathcal{E}(\theta), d\theta \right\rangle$$

$$\leq \hat{\mathcal{E}}(\theta, \epsilon_2) + \int_\theta^{\theta'} \|\nabla_\theta \hat{\mathcal{E}}(\theta, \epsilon_2) - \nabla_\theta \mathcal{E}(\theta)\|\|d\theta\| + \mathcal{E}(\theta') - \mathcal{E}(\theta)$$

$$\leq \hat{\mathcal{E}}(\theta, \epsilon_2) + \mathbf{O}(\epsilon_2^{1-6\eta})\|d^{(1)}\|\alpha - c\|\nabla_\theta \mathcal{E}(\theta)\|\alpha\epsilon_6$$

$$= \hat{\mathcal{E}}(\theta, \epsilon_2) + \|\nabla_\theta \mathcal{E}(\theta)\|\alpha(\mathbf{O}(\epsilon_2^{1-6\eta}) - c\epsilon_6).$$

As long as $\eta < 1/6$, we can choose sufficiently small ϵ_2 such that $\hat{\mathcal{E}}(\theta', \epsilon_2) < \hat{\mathcal{E}}(\theta, \epsilon_2)$. Since we assume there are infinitely many subdivisions and Corollary IX.5 shows that line search Algorithm 3 will always terminate finitely, we conclude that Algorithm 1 will generate an infinite sequence θ of decreasing $\hat{\mathcal{E}}(\theta, \epsilon_2)$ for sufficiently small ϵ_2. Further, each θ is safe and each $\hat{\mathcal{E}}(\theta, \epsilon_2)$ is finite by the motion bound. But these properties contradict Lemma IX.6. □

X. Using Algorithm 1 as SIP Solver

We show that Algorithm 1 is indeed a solver of the SIP problem Equation (1). To this end, we consider running Algorithm 1 for an infinite number of iterations and we use superscript to denote iteration number. At the kth iteration, we use $\mu = \mu^k, \epsilon_d = \epsilon_d^k$ and we assume the sequences $\{\mu^k\}$ and $\{\epsilon_d^k\}$ are both null sequences. This will generate a sequence of solutions $\{\theta^k\}$ and we consider one of its convergent subsequence also denoted as $\{\theta^k\} \to \theta^0$. We consider the first-order optimality condition at θ^0:

Definition X.1. *If θ^0 satifies the first-order optimality condition, then for each direction D_θ such that:*

$$\left\langle D_\theta, \nabla_\theta dist(b_{ij}(t,\theta^0), o_k) \right\rangle \geq 0 \quad \forall dist(b_{ij}(t,\theta^0), o_k) = 0,$$

we have $\left\langle D_\theta, \nabla_\theta \mathcal{O}(\theta^0) \right\rangle \geq 0$.

We further assume the following generalized Mangasarian-Fromovitz constraint qualification (GMFCQ) holds at θ^0:

Assumption X.2. *There exists some direction D_θ and positive ϵ_7 such that:*

$$\left\langle D_\theta, \nabla_\theta dist(b_{ij}(t,\theta^0), o_k) \right\rangle \geq \epsilon_7 \quad \forall dist(b_{ij}(t,\theta^0), o_k) = 0.$$

MFCQ is a standard assumption establishing connection between the first-order optimality condition of NLP and the gradient of the Lagrangian function. Our generalized version of MFCQ requires a positive constant ϵ_7, which is essential for extending it to SIP. Note that GMFCQ is equivalent to standard MFCQ for NLP. We start by showing a standard consequence of assuming GMFCQ:

Lemma X.3. *Taking Assumption X.2, if first-order optimality fails at a trajectory θ^0, then we have a direction D_θ such that:*

$$\left\langle D_\theta, \nabla_\theta \mathcal{O}(\theta^0) \right\rangle < -\epsilon_8$$
$$\left\langle D_\theta, \nabla_\theta dist(b_{ij}(t,\theta^0), o_k) \right\rangle > \epsilon_9 \quad \forall dist(b_{ij}(t,\theta^0), o_k) = 0.$$

Proof. Under our assumptions, there is a direction D_θ^1 satisfying GMFCQ and another direction D_θ^2 violating first-order optimality condition. We can then consider a third direction $D_\theta^3 = D_\theta^1 \epsilon_{10} + D_\theta^2$ where we have:

$$\left\langle D_\theta^3, \nabla_\theta \mathcal{O}(\theta^0) \right\rangle = \epsilon_{10} \left\langle D_\theta^1, \nabla_\theta \mathcal{O}(\theta^0) \right\rangle - \epsilon_{11}$$
$$\left\langle D_\theta^3, \nabla_\theta dist(b_{ij}(t,\theta^0), o_k) \right\rangle \geq \epsilon_{10}\epsilon_7,$$

where ϵ_{11} is some positive constant. We can thus choose sufficiently small ϵ_{10} to make the righthand side of the first equation negative and the righthand side of the second one positive. $\square$

Assuming a failure direction D_θ^3 exists, we now start to show that the directional derivative of our objective function $\mathcal{E}$ along D_θ^3 is bounded away from zero, which contradicts the fact that our gradient norm threshold $\{\epsilon_d^k\}$ is tending to zero. To bound the derivative near θ^0, we need to classify $b_{ij}(t,\theta^0)$ into two categories: 1) its distance to o is bounded away from zero; 2) its distance to o is close to zero but b_{ij} is moving away along D_θ^3. This result is formalized below:

Lemma X.4. *Taking Assumption III.1, for D_θ^3 stated in Lemma X.3 and each tuple of $\langle i,j,k \rangle$, one of the following conditions holds:*

$$dist(b_{ij}(t,\theta^0), o_k) > \epsilon_{12}$$
$$dist(b_{ij}(t,\theta^0), o_k) \leq \epsilon_{12} \wedge \left\langle D_\theta^3, \nabla_\theta dist(b_{ij}(t,\theta^0), o_k) \right\rangle \geq \frac{\epsilon_9}{2},$$

where ϵ_{12} is some positive constant.

Proof. Suppose otherwise, for arbitrarily small ϵ_{12}, we can find some i,j,k,t such that:

$$\begin{aligned} dist(b_{ij}(t,\theta^0), o_k) \leq \epsilon_{12}\wedge \\ \left\langle D_\theta^3, \nabla_\theta dist(b_{ij}(t,\theta^0), o_k) \right\rangle < \frac{\epsilon_9}{2}. \end{aligned} \tag{11}$$

We can construct a sequence of $\{\langle i,j,k,t,\epsilon_{12} \rangle\}$ with diminishing ϵ_{12} such that Equation (11) holds for each $\langle i,j,k,t,\epsilon_{12} \rangle$ tuple. If the sequence is finite, then there must be some:

$$dist(b_{ij}(t,\theta^0), o_k) = 0 \wedge \left\langle D_\theta^3, \nabla_\theta dist(b_{ij}(t,\theta^0), o_k) \right\rangle < \frac{\epsilon_9}{2},$$

contradicting Lemma X.3. If the sequence is infinite, then by Assumption III.1, there is an infinite subsequence with $\langle i,j,k \rangle$ being the same throughout the subsequence. We denote the subsequence as: $\{\langle t,\epsilon_{12} \rangle\}$, which tends to $\{\langle t^0, 0 \rangle\}$. By the continuity of functions we have:

$$dist(b_{ij}(t^0,\theta^0), o_k) = 0 \wedge \left\langle D_\theta^3, \nabla_\theta dist(b_{ij}(t^0,\theta^0), o_k) \right\rangle \leq \frac{\epsilon_9}{2},$$

again contradicting Lemma X.3. $\square$

The above analysis is performed at θ^0. But by the continuity of problem data, we can extend the conditions to a small vicinity around θ^0. We denote $\mathcal{B}(\theta^0, \epsilon_{13})$ as a closed ball around θ^0 with a radius equal to ϵ_{13}. We formalize this observation in the following lemma:

Lemma X.5. *Taking Assumption X.2, III.1, and for D_θ^3 stated in Lemma X.3, we have:*

$$\left\langle D_\theta^3, \nabla_\theta \mathcal{O}(\theta) \right\rangle < -\frac{\epsilon_8}{2},$$

and one of the following condition holds each tuple of $\langle i,j,k \rangle$:

$$dist(b_{ij}(t,\theta), o_k) > \frac{\epsilon_{12}}{2} \tag{12}$$
$$\left\langle D_\theta^3, \nabla_\theta dist(b_{ij}(t,\theta), o_k) \right\rangle \geq \frac{\epsilon_9}{4}, \tag{13}$$

for any $\theta \in \mathcal{B}(\theta^0, \epsilon_{13})$.

Proof. Combining Lemma X.3, X.4, and the continuity of problem data. $\square$

Lemma X.5 allows us to quantify the gradient norm of $\mathcal{E}(\theta, \mu)$ (we write μ as an additional parameter of $\mathcal{E}$ for convenience). The gradient norm should tend to zero as $k \to \infty$. However, Lemma X.5 would bound it away from zero, leading to a contradiction.

Lemma X.6. *Taking Assumption X.2, III.1, IV.1, suppose $\{\mu^k\}$ is a null sequence, and for D_θ^3 stated in Lemma X.3, there exists a D_θ^3 and sufficiently large k such that for any $\theta \in \mathcal{B}(\theta^0, \epsilon_{14})$:*

$$\left\langle D_\theta^3, \nabla_\theta \mathcal{E}(\theta, \mu^k) \right\rangle < -\epsilon_{15},$$

for some positive constant ϵ_{14}.

Proof. The gradient consists of three sub-terms:

$$\nabla_\theta \mathcal{E}(\theta, \mu^k) = \nabla_\theta \mathcal{O}(\theta) + \nabla_\theta \bar{\mathcal{P}}_1(\theta, \mu^k) + \nabla_\theta \bar{\mathcal{P}}_2(\theta, \mu^k)$$

$$\bar{\mathcal{P}}_1(\theta, \mu^k) \triangleq \mu^k \sum_{ijkl}^{I} (T_1^l - T_0^l) \mathcal{P}_{ijkl}$$

$$\bar{\mathcal{P}}_2(\theta, \mu^k) \triangleq \mu^k \sum_{ijkl}^{II} (T_1^l - T_0^l) \mathcal{P}_{ijkl}.$$

Here we use $\sum_{ijkl}^{I}$ to denote a summation over terms $\mathcal{P}_{ijkl}$ where Equation (12) holds and $\sum_{ijkl}^{II}$ denotes a summation where Equation (12) does ont hold but Equation (13) holds. From Lemma X.5, we have the following holds for the first two terms:

$$\left\langle D_\theta^3, \nabla_\theta \mathcal{O}(\theta) \right\rangle < -\frac{\epsilon_8}{2} \quad \left\langle D_\theta^3, \nabla_\theta \bar{\mathcal{P}}_2(\theta, \mu^k) \right\rangle < 0.$$

The third term can be arbitrarily small for sufficiently large k because:

$$\left| \left\langle D_\theta^3, \nabla_\theta \bar{\mathcal{P}}_1(\theta, \mu^k) \right\rangle \right|$$

$$\leq \mu^k \sum_{ijkl}^{I} (T_1^l - T_0^l) \left| \left\langle D_\theta^3, \left. \frac{\partial \mathcal{P}(x)}{\partial x} \right|_{\epsilon_{12}/2} \nabla_\theta \bar{\text{dist}} \right\rangle \right|$$

$$\leq \mu^k T \left| \left. \frac{\partial \mathcal{P}(x)}{\partial x} \right|_{\epsilon_{12}/2} \right| \left| \left\langle D_\theta^3, \nabla_\theta \bar{\text{dist}} \right\rangle \right|.$$

Here we have used Assumption IV.1 and denote $\nabla_\theta \bar{\text{dist}}$ as the location on trajectory where $\left| \left\langle D_\theta^3, \nabla_\theta \bar{\text{dist}} \right\rangle \right|$ takes the maximum value. Since $\{\mu^k\}$ is a null sequence, the third term can be arbitrarily small and the lemma follows. □

We are now ready to prove our main result:

Proof of Theorem V.3. Suppose otherwise, i.e. the first-order optimality condition fails, then the condition of Lemma X.6 holds, indicating that $\|\nabla_\theta \mathcal{E}(\theta^k, \mu^k)\|_\infty$ is bounded away from zero. But this contradicts the fact that $\{\epsilon_d^k\}$ is null. □